

3D Collapse of Rotating Stellar Iron Cores in General Relativity with Microphysics

C. D. Ott,¹ H. Dimmelmeier,² A. Marek,² H.-T. Janka,² I. Hawke,³ B. Zink,^{2,4} and E. Schnetter⁴

¹Max-Planck-Institut für Gravitationsphysik, Albert-Einstein-Institut, Am Mühlenberg 1, D-14476 Potsdam, Germany

²Max-Planck-Institut für Astrophysik, Karl-Schwarzschild-Strasse 1, D-85741 Garching, Germany

³School of Mathematics, University of Southampton, Southampton SO17 1BJ, UK

⁴Center for Computation and Technology, Louisiana State University, Baton Rouge, LA 70803, USA

We present results from the first 2D and 3D simulations of the collapse of rotating stellar iron cores in general relativity employing a finite-temperature equation of state and an approximate treatment of deleptonization during collapse. We compare fully nonlinear and conformally flat spacetime evolution methods and find that the conformally flat treatment is sufficiently accurate for the core-collapse supernova problem. We focus on the gravitational wave (GW) emission from rotating collapse, core bounce, and early postbounce phases. Our results indicate that the GW signature of these phases is much more generic than previously estimated. In addition, we track the growth of a nonaxisymmetric instability of dominant $m = 1$ character in one of our models that leads to prolonged narrow-band GW emission at ~ 930 Hz over several tens of milliseconds.

PACS numbers: 04.25.Dm, 04.30.Db, 95.30.Sf, 97.60.Bw

Introduction.—For more than two decades astrophysicists have struggled to compute the gravitational wave (GW) signal produced by rotating stellar core collapse and the subsequent supernova evolution. Besides the coalescence of black hole and neutron star binaries, core-collapse events are considered to be among the most promising sources of detectable GWs. Theoretical predictions are still hampered by three major problems: (i) The rotational configuration prior to gravitational collapse is still uncertain since multi-D evolutionary calculations of rotating massive stars have not yet been performed; (ii) reliable waveform estimates require a general relativistic (GR) treatment, since both high densities and velocities in combination with strong gravitational fields are encountered in this problem; and (iii) an adequate treatment of the nuclear equation of state (EOS) and the neutrino microphysics/radiative transfer is crucial for obtaining realistic collapse, bounce, and postbounce dynamics and waveforms. GW emission from core-collapse supernovae may arise from rotating collapse and bounce, postbounce neutrino-driven convection, anisotropic neutrino emission, nonaxisymmetric rotational instabilities of the protoneutron star (PNS), or from the recently proposed PNS core g-mode oscillations. Previous estimates of the GW signature of core-collapse supernovae have either relied on Newtonian simulations [1, 2, 3, 4, 5, 6] (to some extent approximating GR effects [7]) or GR simulations with simplified analytic (so-called hybrid) EOSs and no neutrino treatment [8, 9, 10, 11]. Depending on the rotation strength, softness of the EOS at subnuclear densities, and inclusion of GR effects, the collapse dynamics and accordingly the GW signature can differ significantly.

Here we present new results from GR simulations, focussing on the rotating collapse, bounce, and early postbounce phases. These are the *first-ever* multi-D simulations in GR with presupernova models from stellar evolu-

tion calculations, a finite-temperature nuclear EOS, and a simple, but effective treatment of electron capture and neutrino radiation effects during collapse. In this way we obtain the most accurate estimates of the GW signature of rotating stellar core collapse in full GR to date.

Method and Initial Models.—We perform all 3D simulations in full 3+1 GR using the CACTUS infrastructure [12], Cartesian coordinates, and mesh refinement provided by the CARPET driver [13]. The only assumption on symmetry is reflection invariance with respect to the equatorial plane. Spacetime is evolved using the BSSN formulation (see, e.g., [14]) and we fix the gauge freedom by 1+log slicing and by a hyperbolic shift condition similar to minimal distortion [15]. We use the hydrodynamics code WHISKY [16], which implements the equations of GR hydrodynamics via finite-volume methods. Typical simulation grids extend to 3000 km and use 9 refinement levels. The central resolution is ~ 350 m. In addition, we perform axisymmetric (2D) simulations for all models using the CoCoNUT code [8, 17], which approximates GR by the conformal flatness condition (CFC). CoCoNUT utilizes spherical coordinates with 200 logarithmically spaced radial and 30 equidistant angular zones, covering 90° , and a central resolution of ~ 400 m. We extract GWs from the mass motions using a variant of the Newtonian quadrupole formula [9].

We employ the finite-temperature nuclear EOS of Shen et al. [18] in the implementation of Marek et al. [19] in both codes. Deleptonization by electron captures on nuclei and free protons is realized as proposed and tested by Liebendörfer [20]: The electron fraction Y_e is parameterized as a function of density during collapse based on data from spherically symmetric radiation-hydrodynamics simulations using standard electron capture rates [19]. After core bounce, Y_e is passively advected and further lepton loss is neglected, but neutrino pressure contributions continue to be taken into account

TABLE I: Model summary. ρ_b is the density at bounce, the maximum characteristic GW strain $h_{\text{char,max}}$ is at a distance of 10 kpc, and E_{gw} is the energy emitted in GWs. Values for model E20A_{pb} include the GW emission from nonaxisymmetric structures for 70 ms postbounce evolution time.

Model	A [10^8 cm]	β_i [%]	β_b [%]	ρ_b [10^{14} g/cm ³]	$h_{\text{char,max}}$ [10^{-21}]	E_{gw} [$10^{-9} M_\odot c^2$]
s20A1B1	50.0	0.25	0.90	3.29	1.46	0.6
s20A1B5	50.0	4.00	10.52	2.90	9.68	26.9
s20A2B2	1.0	0.50	6.72	3.07	8.77	22.0
s20A2B4	1.0	1.80	16.33	2.35	4.28	9.4
s20A3B3	0.5	0.90	16.57	2.33	4.58	12.4
E20A	—	0.37	11.31	2.79	12.18	36.9
E20A _{pb}	—	—	—	—	24.23	75.4

above trapping density [20].

In this study we focus on the collapse of massive presupernova iron cores with at most moderate differential rotation, and rotation rates that may be too fast to match garden-variety pulsar birth spin estimates [21, 22], but could be relevant in the collapsar-type gamma-ray burst context [23]. As initial data we use the non-rotating $20 M_\odot$ presupernova model s20 of Woosley et al. [24] which we force to rotate according to the rotation law discussed in [5, 8]. We parameterize our models in terms of the differential rotation parameter A and the initial ratio of rotational kinetic to gravitational binding energy $\beta_i = T/|W|$. In addition, we perform a calculation with the $20 M_\odot$ model E20A of Heger et al. [25], which was evolved to the onset of collapse with a 1D treatment of rotation. In Table I we summarize the model parameters.

Results.—In Fig. 1 we compare GW signals computed with CoCoNut in 2D-CFC and those computed with our 3D-full-GR approach. Model s20A2B2 (red lines) is a moderate rotator with a $\beta_i = 0.50\%$, rotating rigidly in its central region. It stays axisymmetric throughout its numerical evolution. The agreement of 2D-CFC with 3D-full-GR is excellent for this model: Both waveforms match almost perfectly at bounce and during the very early postbounce phase. A few ms after bounce, when convection in the region behind the stalling shock sets in due to a negative entropy gradient, the signals begin to differ quantitatively while remaining in phase. We attribute this small mismatch to the choice of coordinate grids and to differences in the growth and scale of vortical postbounce motions between 2D and 3D. Model s20A1B5 rotates with constant Ω in the entire core. Despite its very large $\beta_i = 4\%$ it remains essentially axisymmetric during the time covered by our simulation, since most of its angular momentum is attached to material at large radii that falls inward and spins up only slowly. The waveforms in CFC and full GR agree very well. Again, both waveforms match best for the strong burst related to core bounce during which more than $\sim 90\%$ of the total GW energy are emitted in an axisymmetric model. The

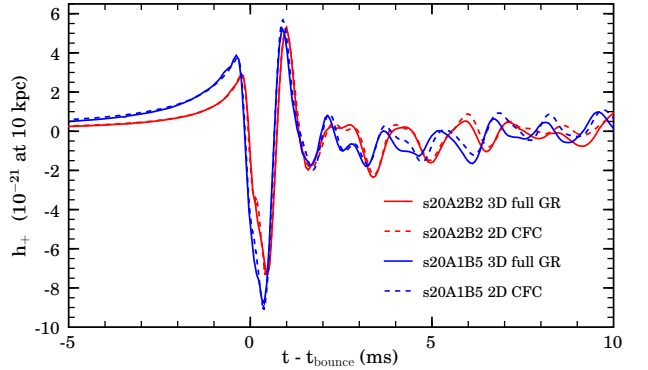


FIG. 1: GW strain h_+ along the equator for models s20A2B2 and s20A1B5. We compare 2D-CFC and 3D-full-GR results.

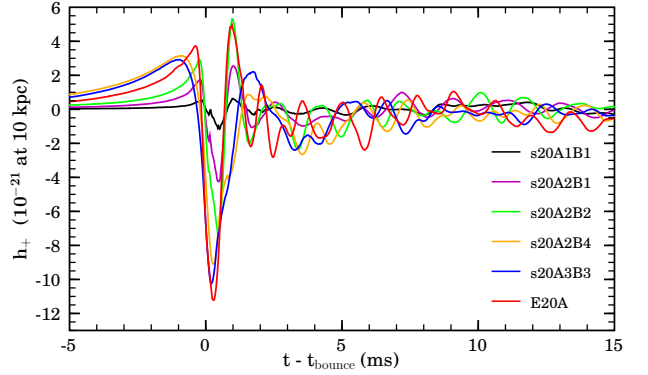


FIG. 2: GW strain h_+ along the equator for all models.

overall excellent agreement of CFC with full GR confirms results of [9, 11] and proves that CFC is a very good approximation to full GR in the core-collapse scenario.

In Fig. 2 we present waveforms of models with varying initial degree of differential rotation A and rotation rate β_i . We find that the inclusion of a microphysical finite-temperature EOS and of electron capture during collapse yields results that differ considerably from those obtained in previous, less sophisticated studies. Fig. 2 exemplifies that largely independent of the initial rotational configuration, the GW signal of the core bounce in rotating collapse has a *generic shape*: a slow signal increase in the pre-bounce phase, a large negative amplitude at core bounce when the motion of the quasi-homologously collapsing inner core is reversed, followed by a ring-down. This so-called “Type I” signature corresponds to a baryonic pressure dominated bounce [1, 2, 5, 8]. Thus all our models undergo core bounce dominated by the stiffening of the EOS at nuclear density.

This is in stark contrast to the studies using the hybrid EOS [2, 8, 9, 10], where initial models with rotation rates in the range investigated here develop sufficient centrifugal support during contraction to stop collapse at subnuclear densities, resulting in several consecutive centrifugal bounces separated by phases of coherent re-expansion of the inner core. While in GR models exhibit-

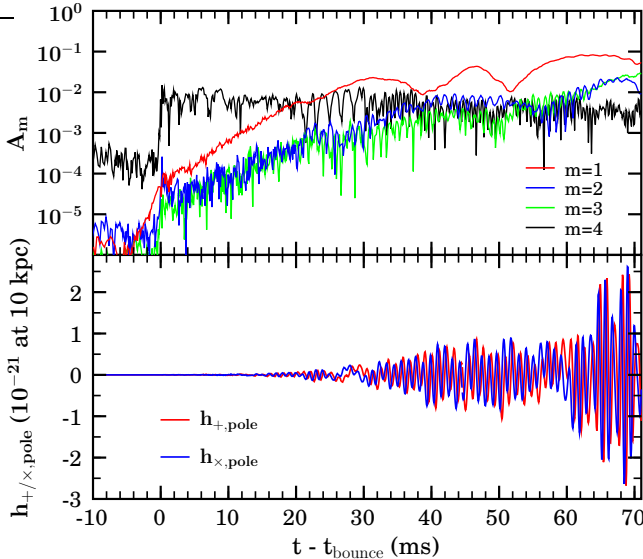


FIG. 3: Normalized mode amplitudes A_m at postbounce times (upper panel) and GW strains h_+ and h_x along the poles (lower panel) for model E20A.

ing such multiple centrifugal bounce and the corresponding ‘‘Type II’’ GW signals are only rarer compared to Newtonian gravity [8], we do not observe *any* such model in this study. An evident example is model s20A2B4: In previous studies without detailed microphysics, the corresponding model with identical initial rotation parameters (A2B4G1) showed clear ‘‘Type II’’ behavior in both Newtonian and GR calculations [2, 8].

The suppression of the multiple centrifugal bounce scenario is due to two physical effects: (i) In contrast to the simple hybrid EOS, in our case the mass and dynamics of the inner core (which is most important for the GW emission) is not merely determined by the adiabatic index $\gamma = d \ln P / d \ln \rho$ (at constant entropy) of the EOS, but also by deleptonization during collapse. This leads to *considerably smaller inner cores with less angular momentum and weaker pressure support*. (ii) Since multiple centrifugal bounce was observed for a model with initially moderately fast rotation in a previous Newtonian study [1] where both a microphysical finite-temperature EOS and a deleptonization scheme were employed, the absence of this collapse type in our study is not only caused by microphysical effects, but also by the effectively *stronger* gravity in GR. This is in accordance with simulations using the simple hybrid EOS [8]. A detailed analysis of the interplay and quantitative influence of the above two effects responsible for the elimination of multiple centrifugal bounce in the rotational stellar core-collapse scenario will be presented in a future publication.

Model E20A possesses the largest GW amplitude of all our models. In addition, it reaches a high β_b at core bounce (see Table I) and settles at a postbounce β_f of $\sim 9\%$. In a previous Newtonian 3D study, Ott et al. [26] have found a low- $T/|W|$ nonaxisymmetric in-

stability for a PNS with similar β_f . In order to verify their findings, we trace the evolution of model E20A to 70 ms after bounce and perform an analysis of azimuthal density modes $\propto e^{im\varphi}$ in the equatorial plane by computing complex Fourier amplitudes $C_m = \frac{1}{2\pi} \int_0^{2\pi} \rho(\varpi, \varphi, z=0) e^{im\varphi} d\varphi$ on rings of constant coordinate radius. In the top panel of Fig. 3 we display the normalized mode amplitudes $A_m = \frac{|C_m|}{C_0}$ extracted at 15 km radius. Without adding artificial seed perturbations to model E20A, discretization errors trigger $m = \{1, 2, 3\}$ modes, which rise to a level of $\sim 10^{-5}$ during the ~ 220 ms collapse phase. Shortly after bounce, the $m = 1$ mode begins to grow at a significant rate. This growth on a dynamical time scale, lasting over tens of ms until saturation, is closely followed by a growth of $m = \{2, 3\}$ daughter modes [26, 27]. Note that the $m = 4$ Cartesian grid mode starts out on the $\sim 10^{-4}$ level and remains constant until the plunge phase of collapse during which all modes are amplified. After core bounce, model E20A remains dynamically stable to the $m = 4$ grid mode. In the lower panel of Fig. 3 we plot the GW strains h_+ and h_x as seen along the polar axis. The rotational symmetry of E20A before and early after bounce times is reflected in the fact that h_+ and h_x are practically zero until E20A develops considerable nonaxisymmetry at ~ 25 ms after bounce when the $m = 1$ mode becomes dominant and its $m = 2$, GW-emitting harmonic reaches a sizable amplitude. In remarkable agreement with expectations for a spinning bar, h_+ and h_x oscillate at the same frequency (~ 930 Hz) and are phase-shifted by a quarter cycle.

Discussion.—Our results indicate that the GW signature of the collapse, core bounce, and early postbounce phases of the core-collapse supernova evolution is much more generic than previously thought. We find that the dynamics of core bounce are mainly dominated by gravity and microphysics, reducing the importance of centrifugal support for the rotation rates considered here. Importantly, for our model set we do not observe rotationally induced multiple core bounce at subnuclear density as proposed by previous studies that did not include a microphysical finite-temperature EOS and electron capture treatment in combination with GR. Thus we predict that the core-bounce waveform of models in a large parameter space of initial rotation rate and degree of differential rotation will likely both qualitatively and quantitatively resemble those presented in Fig. 2.

Model E20A, which we evolve to later postbounce times, exhibits the dynamical growth of a nonaxisymmetric low- $T/|W|$ corotation-type $m = 1$ instability [26, 27, 28]. We also find $m = \{2, 3\}$ contributions and thus significant GW emission from the quadrupole components of these modes. We emphasize that we observe this instability not only in E20A, but also in other models with comparable values of β_f . Our results, which remove the limitations of previous studies [10, 26, 29, 30],

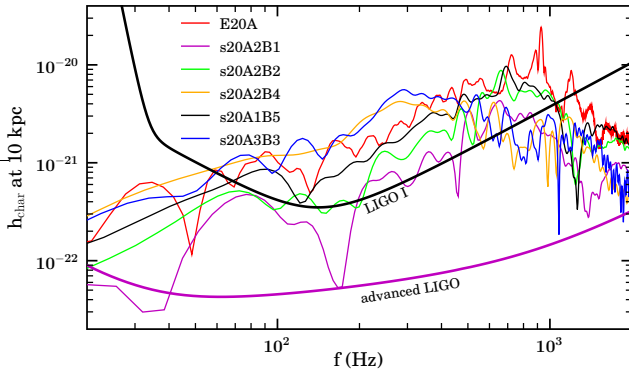


FIG. 4: Spectra of the characteristic GW strain h_{char} of all models and the LIGO (optimal) rms noise curves [31].

demonstrate that the development of nonaxisymmetric structures is neither limited to Newtonian gravity, simple matter models, equilibrium configurations, nor high values of β above the classical thresholds for the onset of nonaxisymmetric instabilities, but may rather be a phenomenon occurring generically in differentially rotating compact stars.

For the GW signals from the axisymmetric collapse and core-bounce phase we obtain peak amplitudes of up to $h \sim 10^{-20}$ at 10 kpc, while the nonaxisymmetric structures in model E20A developing later emit GWs with h only a factor ~ 5 smaller. However, since the latter emission process operates over several tens of ms, the total energy E_{gw} emitted in GWs is *larger* than that from the core-bounce signal. This is evident in Fig. 4, where we display the characteristic GW strain spectra $h_{\text{char}} = R^{-1} \sqrt{2\pi^{-2} dE_{\text{gw}}/df}$ [5] for all models, evolving E20A for 70 ms after bounce (see also Table I). Considering only the core-bounce waveforms, h_{char} has its maximum between 300 and 800 Hz, while for model E20A it peaks at ~ 930 Hz, the pattern frequency of the GW-emitting component of its nonaxisymmetric structures. We conclude that the core-bounce GW signals of all models investigated here should be detectable by current and future LIGO-class detectors from anywhere in the Milky Way. Models that develop nonaxisymmetric instabilities may be detectable out to much larger distances if the instability persists for a sufficiently long time.

We point out that due to the nature of the approximation used for the neutrino effects in this study, we can only accurately model the GW emission in the collapse, bounce, and early postbounce epoch of the core-collapse supernova scenario, but not much later than the neutrino burst at shock breakout a few ms after bounce. In future work we plan to improve upon this and carry out longer-term postbounce evolutions, where additional GW emission mechanisms may play an important role [6, 7].

We thank A. Burrows, E. Müller, S. Ou, L. Rezzolla, E. Seidel, D. Shoemaker, N. Stergioulas, and J. Tohline for help and stimulating discussions. This research was

partially supported by the DFG (SFB/Transregio 7) and by the NCSA under grant No. AST050022N.

- [1] R. Mönchmeyer, G. Schäfer, E. Müller, and R. Kates, *Astron. Astrophys.* **246**, 417 (1991).
- [2] T. Zwerger and E. Müller, *Astron. Astrophys.* **320**, 209 (1997).
- [3] M. Rampp, E. Müller, and M. Ruffert, *Astron. Astrophys.* **332**, 969 (1998).
- [4] K. Kotake, S. Yamada, K. Sato, K. Sumiyoshi, H. Ono, and H. Suzuki, *Phys. Rev. D* **69**, 124004 (2004).
- [5] C. D. Ott, A. Burrows, E. Livne, and R. Walder, *Astrophys. J.* **600**, 834 (2004).
- [6] C. D. Ott, A. Burrows, L. Dessart, and E. Livne, *Phys. Rev. Lett.* **96**, 201102 (2006).
- [7] E. Müller, M. Rampp, R. Buras, H.-T. Janka, and D. H. Shoemaker, *Astrophys. J.* **603**, 221 (2004).
- [8] H. Dimmelmeier, J. A. Font, and E. Müller, *Astron. Astrophys.* **388**, 917 (2002), *ibid.* **393**, 523 (2002).
- [9] M. Shibata and Y.-I. Sekiguchi, *Phys. Rev. D* **69**, 084024 (2004).
- [10] M. Shibata and Y.-I. Sekiguchi, *Phys. Rev. D* **71**, 024014 (2005).
- [11] P. Cerdá-Durán, G. Faye, H. Dimmelmeier, J. A. Font, J. M. Ibáñez, E. Müller, and G. Schäfer, *Astron. Astrophys.* **439**, 1033 (2005).
- [12] <http://www.cactuscode.org>.
- [13] E. Schnetter, S. H. Hawley, and I. Hawke, *Class. Quantum Grav.* **21**, 1465 (2004).
- [14] T. W. Baumgarte and S. L. Shapiro, *Phys. Rep.* **376**, 41 (2003).
- [15] M. Shibata, *Astrophys. J.* **595**, 992 (2003).
- [16] L. Baiotti, I. Hawke, P. J. Montero, F. Löffler, L. Rezzolla, N. Stergioulas, J. A. Font, and E. Seidel, *Phys. Rev. D* **71**, 024035 (2005).
- [17] H. Dimmelmeier, J. Novak, J. A. Font, J. M. Ibáñez, and E. Müller, *Phys. Rev. D* **71**, 064023 (2005).
- [18] H. Shen, H. Toki, K. Oyamatsu, and K. Sumiyoshi, *Prog. Theor. Phys.* **100**, 1013 (1998).
- [19] A. Marek, H.-T. Janka, R. Buras, M. Liebendörfer, and M. Rampp, *Astron. Astrophys.* **443**, 201 (2005).
- [20] M. Liebendörfer, *Astrophys. J.* **633**, 1042 (2005).
- [21] A. Heger, S. E. Woosley, and H. C. Spruit, *Astrophys. J.* **626**, 350 (2005).
- [22] C. D. Ott, A. Burrows, T. A. Thompson, E. Livne, and R. Walder, *Astrophys. J. Suppl. Ser.* **164**, 130 (2006).
- [23] S. E. Woosley and A. Heger, *Astrophys. J.* **637**, 914 (2006).
- [24] S. E. Woosley, A. Heger, and T. A. Weaver, *Rev. Mod. Phys.* **74**, 1015 (2002).
- [25] A. Heger, N. Langer, and S. E. Woosley, *Astrophys. J.* **528**, 368 (2000).
- [26] C. D. Ott, S. Ou, J. E. Tohline, and A. Burrows, *Astrophys. J. Lett.* **625**, L119 (2005).
- [27] S. Ou and J. Tohline, *Astrophys. J.* (2006), accepted.
- [28] M. Saijo and S. Yoshida, *Mon. Not. R. Astron. Soc.* **368**, 1429 (2006).
- [29] J. M. Centrella, K. C. B. New, L. L. Lowe, and J. D. Brown, *Astrophys. J. Lett.* **550**, L193 (2001).
- [30] M. Shibata, S. Karino, and Y. Eriguchi, *Mon. Not. R. Astron. Soc.* **334**, L27 (2002).
- [31] D. H. Shoemaker, private communication (2006).